which should be cited to refer to this work.

Spherical aromaticity of Jahn–Teller active fullerene ions

Marko Perić · Ljubica Andjelković · Matija Zlatar · Aleksandar S. Nikolić · Claude Daul · Maja Gruden-Pavlović

Abstract Density functional theory was applied to compute the nucleus-independent chemical shifts of fullerene (C_{60}), the fullerene ion C_{60}^{10+}, and the Jahn–Teller active fullerene anion C_{60}^{-} and cation C_{60}^{+}. Positioning a ^{3}He nucleus inside the cage of each of these fullerene species facilitates investigations of the substantial differences among them, ^{3}He NMR chemical shifts can provide important data on the aromatic behavior of these molecular cages. Thus, we also calculated the NMR chemical shift of a ^{3}He atom positioned at the center of each fullerene species investigated (C_{60}, C_{60}^{10+}, C_{60}^{-}, and C_{60}^{+}). The data obtained revealed significant differences in the aromatic behavior of the C_{60} (moderately aromatic) and C_{60}^{10+} (highly aromatic) species. The values of the nucleus-independent chemical shift parameters were also scanned along the intrinsic distortion path for the C_{60}^{-} and C_{60}^{+} species. In both cases, antiaromatic character decreases with increasing deviation from high-symmetry structures to low-symmetry global minimum points, resulting in the antiaromatic C_{60}^{-} and weakly aromatic C_{60}^{+}.

Keywords Density functional theory · Spherical aromaticity · Jahn–Teller effect · Fullerene ions

M. Perić · L. Andjelković · M. Zlatar
Center for Chemistry, Institute of Chemistry, Technology, and Metallurgy, University of Belgrade, Studentski Trg 12-16, 11001 Belgrade, Serbia

A. S. Nikolić · M. Gruden-Pavlović (✉)
Faculty of Chemistry, University of Belgrade, Studentski Trg 12-16, 11001 Belgrade, Serbia
e-mail: gmaja@chem.bg.ac.rs

C. Daul
Department of Chemistry, University of Fribourg, Chemin du Musée 9, 1700 Fribourg, Switzerland

Introduction

The well-known concept of aromaticity can be applied not only to planar molecules but also to three-dimensional (3D) spherical species; such aromaticity is termed "spherical aromaticity" [1–6]. According to Hirsch's rule [1–3], spherical structures are aromatic if they have $2(N + 1)^2$ π electrons, where N is an arbitrary positive integer (this rule is analogous to the $4n + 2$ Hückel rule for cyclic annulenes). In the fullerene molecule, π shells are completely filled with $2(N + 1)^2$ electrons, thus implying aromatic character [7]. Moreover, charged fullerenes that obey the $2(N + 1)^2$ rule are even more aromatic than neutral fullerenes [1, 3]. However, structures with partially filled π orbitals demand more extensive examination of their aromaticities because of their violation of the $2(N + 1)^2$ rule. An additional problem arises in species with a degenerate ground state due to the presence of the Jahn–Teller (JT) effect. The JT theorem states that a molecule with a degenerate electronic ground state distorts to a lower-symmetry (LS) point group according to the epikernel principle [8, 9]. This removes the electron degeneracy and lowers the energy. Nevertheless, to the best of our knowledge, only a few studies [10, 11] that deal with the influence of JT distortion on aromatic behavior can be found in the literature. Hence, an examination of spherical aromaticity in JT-active species would be rather interesting and require detailed analysis.

Among the many techniques used to evaluate aromatic character, the nucleus-independent chemical shift (NICS) [12, 13] is certainly the most useful, and it can also be applied to gauge spherical aromaticity. In general, negative and positive NICS values are associated with aromatic and antiaromatic rings. Additionally, helium (^{3}He) NMR chemical shifts have proven to be powerful tools for

probing the interior magnetic fields of cage compounds and gaining data on aromatic behavior [14–21].

In the work described in this paper, in order to explain the relationship between vibronic coupling and spherical aromaticity, NICS values were calculated for the fullerene anion (C_{60}^-) and the fullerene cation (C_{60}^+) (see Fig. 1) along the intrinsic distortion path (IDP) [22–25]. The philosophy of the IDP method is based on the fact that all information on the vibronic coupling for a high-symmetry (HS) nuclear arrangement is also contained in the distorted LS energy minimum structure, which is a true minimum on the potential energy surface [22–25]. NICS parameters were also computed for JT-inactive species for comparison purposes: a neutral fullerene molecule and the charged fullerene C_{60}^{10+}, which are examples of molecules that fulfill the $2(N + 1)^2$ rule (Fig. 1). The NMR chemical shifts of a ^{3}He nucleus positioned in the cavities of C_{60}, C_{60}^{10+}, C_{60}^-, and C_{60}^+ species (i.e., ^{3}He@C_{60}, ^{3}He@C_{60}^{10+}, ^{3}He@C_{60}^-, and ^{3}He@C_{60}^+) were determined in order to gain deeper insight into the origin of aromatic behavior and to elucidate the influence of JT distortion on spherical aromaticity.

Results and discussion

The NICS parameter values for C_{60} (I_h) and C_{60}^{10+} (I_h) structures, as calculated along the C_5, C_3, and C_2 axes of symmetry, from the center of each cage toward the centers of the pentagon and hexagon rings and toward a C–C bond shared by two hexagons, are summarized in Table 1.

It is clear from Table 1 that the pentagons in C_{60} are antiaromatic while the hexagons possess weak aromatic character. Since these opposite aromaticities of five- and six-membered rings practically cancel each other out near the center of the cage, the center is only moderately aromatic. However, the results of previous studies [26, 27] suggest that the precise definition of the aromatic behavior of C_{60} is still unclear.

In contrast to the results of calculations for the neutral fullerene molecule, calculations on the hypothetical C_{60}^{10+} species reveal strong shielding in all possible directions (C_5, C_3, and C_2 axes), as expected [4, 5] (Table 1). The five-membered and six-membered rings in C_{60}^{10+} show a synergistic diatropic (aromatic) effect, so this highly charged fullerene has a large homogeneous magnetic field region.

Adding or removing one electron from neutral C_{60} molecule yields the JT-active C_{60}^- and C_{60}^+ species, respectively (Fig. 1). The fullerene anion has a $^2T_{1u}$ electronic ground state in the icosahedral (I_h) point group, and the decrease in symmetry leads to the D_{3d} global minimum structure with a $^2A_{2u}$ ground electronic state [23]. The ground electronic state of C_{60}^+ in I_h symmetry is ^2H_u. It has been shown that the distortion leads to structures belonging to either the D_{5d} or the D_{3d} point group [28, 29], where the former is the global minimum (our DFT calculations also gave this result). Descent in symmetry from the HS point to the LS conformation leads to the loss of symmetry elements, i.e., a decrease in symmetry from the I_h point group to D_{3d} leads to the loss of the C_5 symmetry axis, while the lowering of symmetry to D_{5d} point group leads to the loss of the C_3 axis. The NICS values of the JT-active fullerene ions were determined along the C_3 and C_2 axes for C_{60}^- and along the C_5 and C_2 axes for C_{60}^+ (Fig. 2).

Calculating the magnetic properties of an open-shell species with a degenerate ground state is still not a straightforward task. To tackle this problem, we evaluated the NICS values of C_{60}^- and C_{60}^+, imposing an HS (I_h) nuclear arrangement and a LS (D_{3d} or D_{5d}, respectively) electron density using the Quild subroutine [30] provided in the ADF 2010.01 program package [11]. NICS values for the C_{60}^- cage at the HS point show strong antiaromatic character in both directions along the C_3 and C_2 axes (Table 2). In the global minimum structure, which has D_{3d} symmetry, paratropic (antiaromatic) character is observed. However, the antiaromatic effect is weaker than it is for the HS structure. Moving toward the surface of C_{60}^- along the

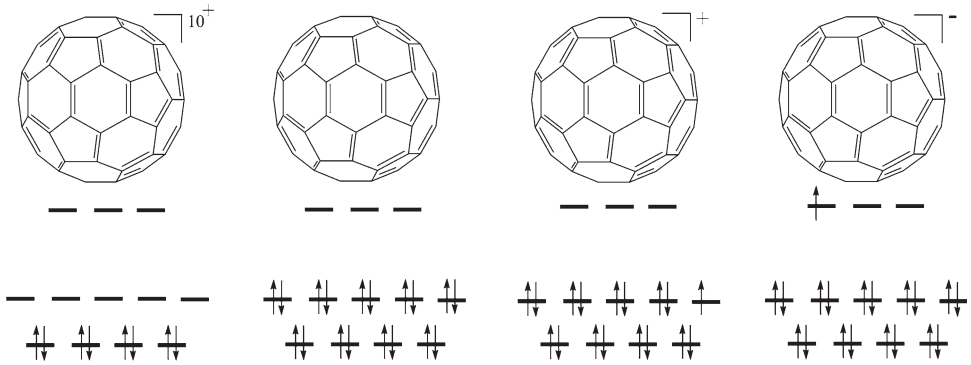

Fig. 1 The molecules studied in this work: simple molecular orbital scheme

Table 1 NICS parameter values (ppm) for C_{60} and C_{60}^{10+}, as calculated along the C_5, C_3, and C_2 axes of symmetry at various distances (d) from the center of the molecule

d/Å	I_h C_{60}				I_h C_{60}^{10+}	
	C_5	C_3	C_2	C_5	C_3	C_2
0	−3.11	−3.11	−3.11	–83.20	–83.20	−83.20
1	−3.07	−3.13	−3.17	–83.20	–86.08	−83.23
2	0.21	−4.19	−4.94	–81.93	–79.81	−82.54
3	12.81	−2.86	–35.14	–45.40	–39.84	−68.44
4	9.09	0.68	–24.50	–12.48	–11.23	−33.94
5	3.32	−0.32	−2.83	−1.01	−1.89	−1.19

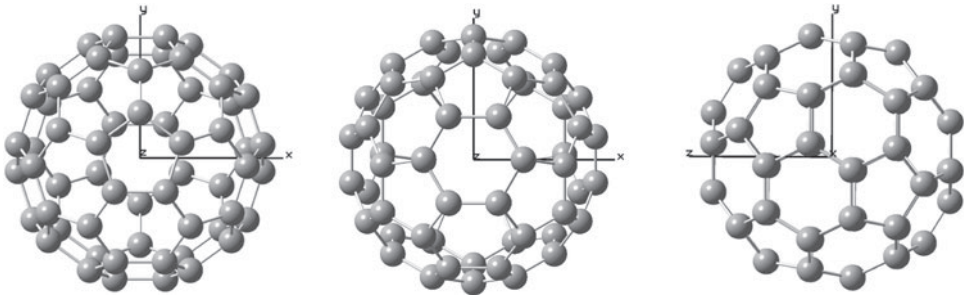

Fig. 2 Rotational axes C_5, C_3, and C_2 in fullerene

Table 2 NICS parameter values (ppm) of the cage compounds C_{60}^- and C_{60}^+ at HS and LS geometries, as calculated along the C_3 and C_2 symmetry axes for C_{60}^- and the C_5 and C_2 axes for C_{60}^+ at various distances (d) from the center of each molecule

d/Å	I_h C_{60}^-		D_{3d} C_{60}^-		I_h C_{60}^+		D_{5d} C_{60}^+	
	C_3	C_2	C_3	C_2	C_5	C_2	C_5	C_2
0	254.84	254.84	22.30	22.30	92.62	92.62	–1.82	–1.82
1	251.93	251.70	21.93	21.08	75.28	102.82	–2.72	–1.28
2	217.78	251.00	17.02	21.30	42.81	140.06	–1.37	–0.55
3	87.51	316.58	4.19	9.46	25.88	107.17	9.88	–24.88
4	11.39	85.42	–0.09	–9.82	10.28	46.06	7.21	–16.13
5	–20.75	57.17	–3.98	5.02	0.46	16.75	1.76	0.58

Table 3 NICS parameter values (ppm) for the global minimum structures of C_{60}^- and C_{60}^+, as calculated at the centers of the pentagon and hexagon rings [NICS (0)] and 1 Å above the center of the ring [NICS (1)]

	D_{3d} C_{60}^-			D_{5d} C_{60}^+		
	NICS (0)	NICS (1)	NICS $(1)_{zz}$	NICS (0)	NICS (1)	NICS $(1)_{zz}$
Pentagon	–18.54	−6.38	–17.55	9.89	5.28	16.39
Hexagon	2.43	−1.46	−3.85	12.60	7.86	24.88

C_3 and C_2 symmetry axes, the antiaromaticity decreases (Table 2). An analysis of local effects leads to the conclusion that the pentagons in a D_{3d} structure have aromatic character, while the hexagons are nonaromatic (Table 3). In order to explain how JT distortion affects the spherical aromaticity, the NICS parameters were scanned along the IDP for the JT-active C_{60}^- species from I_h to the D_{3d} global minimum structure, moving from the center of the cage toward the surface, following the C_3 and C_2 symmetry axes (Figs. 3, 4). As the electron density is not totally symmetric, I_h C_{60}^- possesses strong antiaromatic character. The HOMO–LUMO gap is rather small near the point of electron degeneracy, so the NICS parameters have large values, although they decrease with increasing distortion (Fig. 3). Near the center of the cage, along the first ∼5 % of the path, the NICS values change abruptly, whereas the changes become smoother in the second region. Since the NICS parameter values remain roughly constant near

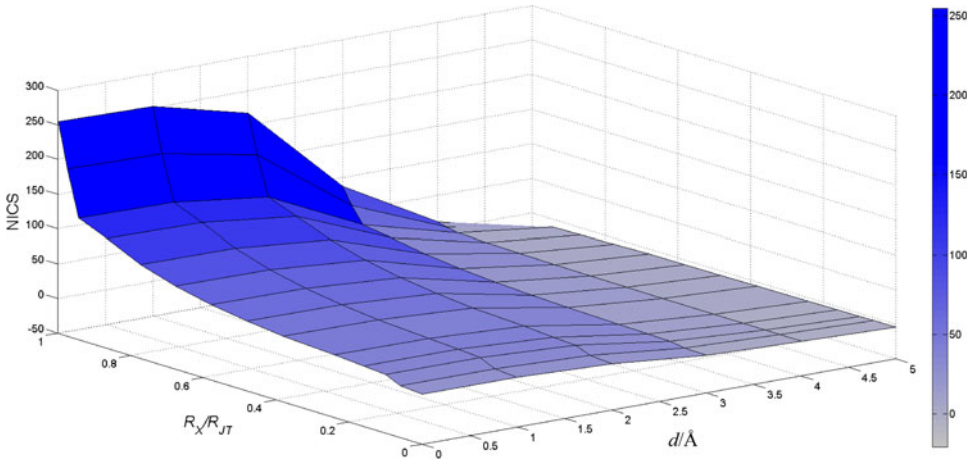

Fig. 3 Schematic plot of NICS values along the C_3 axis of the fullerene anion as a function of the IDP

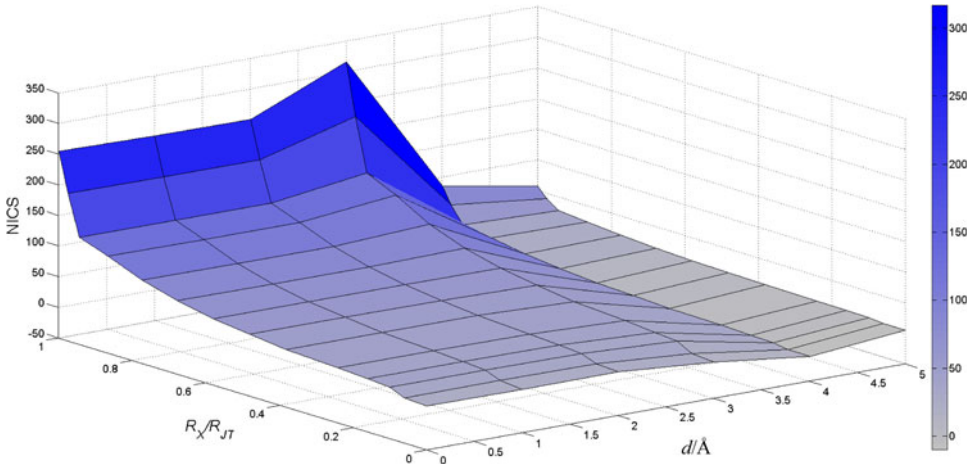

Fig. 4 Schematic plot of the NICS values along the C_2 axis of the fullerene anion as a function of the IDP

the surface of the molecule, the effect of JT distortion on the antiaromaticity is insignificant (Fig. 3). A similar trend was observed upon moving toward the C–C bonds in hexagons (Fig. 4).

Evaluated NICS values for the C_{60}^{+} at its HS point show antiaromatic character, which is more pronounced along the C_2 axis than along the C_5 axis (Table 2). The open-shell icosahedral C_{60}^{-} is somewhat more antiaromatic than icosahedral C_{60}^{+}, as indicated by the NICS values (Table 2). Very weak aromatic character can be observed in the interior of the global minimum structure of the C_{60}^{+} cage, similar to that seen for neutral C_{60}. While moving toward the surface of the molecule along two chosen directions (i.e., the C_5 and C_2 symmetry axes), the same trend is noticed as seen for neutral fullerene. NICS parameter values calculated at the centers of the pentagons and hexagons in the global minimum structure of C_{60}^{+} indicate local antiaromatic character (Table 3). The NICS values were scanned along the IDP, in the directions of the C_5 and C_2 axes (Figs. 5, 6). As can be seen in Fig. 5, the NICS values calculated near the center of the cage change rapidly as a function of the JT distortion, $\vec{R}_X/\vec{R}_{JT}$, along the first 10 % of the path. In the second region, the NICS parameter values gradually decrease toward the global minimum. Moving towards the surfaces of the pentagon rings, JT distortion exerts even less of an influence on the NICS values. Hence, JT distortion only has a significant impact on the aromaticity/antiaromaticity in the interior of C_{60}^{+} along the C_5 axis. Moving along the C_2 symmetry axis (Fig. 6), the opposite effect is observed, in accordance with the results given in Table 2. The largest decrease in NICS values occurs between 2 and 4 Å, where the I_h point (i.e., C_{60}^{+} with I_h geometry and D_{5d} electron density) shows highly antiaromatic character while the global minimum structure is highly aromatic. Evidently, the JT effect strongly affects not only the aromaticity inside the cage but also that near the surfaces of the six-membered rings, in contrast to its effect near the surfaces of the five-membered rings.

The results of an analysis of the ^{3}He NMR isotropic chemical shielding tensor data (Table 4) are in agreement with the results obtained using the NICS methodology. The isotropic chemical shielding tensors of the C_{60} and C_{60}^{10+} minima conformations are positive, indicating that these species have aromatic character. The high positive value of

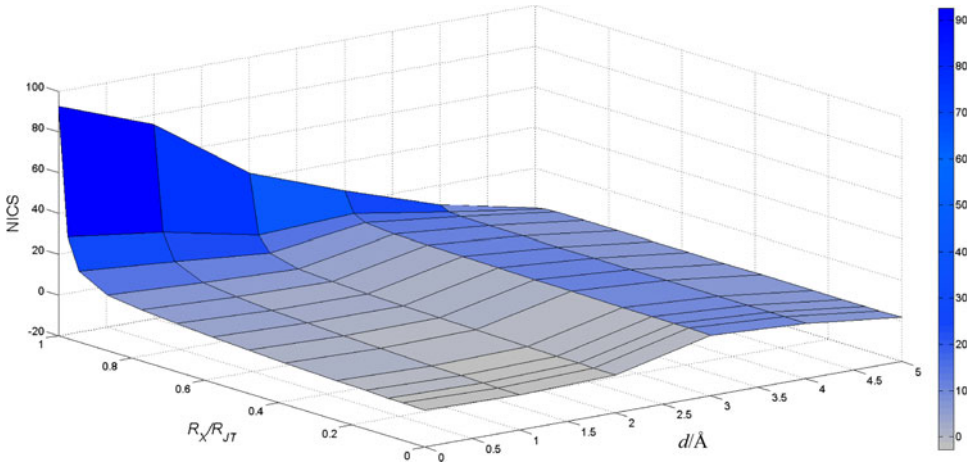

Fig. 5 Schematic plot of NICS values along the C_5 axis of the fullerene cation as a function of the IDP

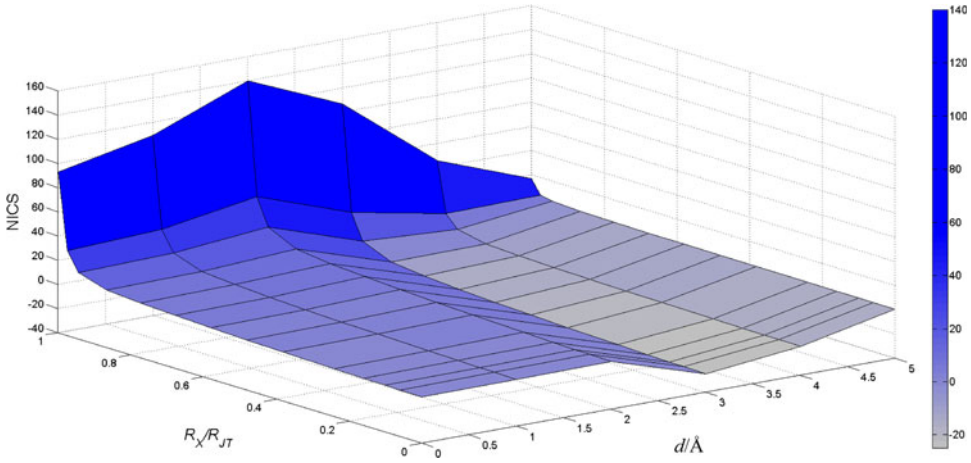

Fig. 6 Schematic plot of the NICS values along the C_2 axis of the fullerene cation as a function of the IDP

Table 4 ^{3}He NMR chemical shielding tensor values (ppm) of the cage compounds C_{60}, C_{60}^{10+}, C_{60}^-, and C_{60}^+ in their HS and LS geometries, as calculated at the center of each molecule

Species	^{3}He NMR chemical shielding tensor/ppm
I_h C_{60}	62.50
I_h C_{60}^{10+}	143.00
I_h C_{60}^-	−194.21
D_{3d} C_{60}^-	37.50
I_h C_{60}^+	−33.88
D_{5d} C_{60}^+	61.17

the ^{3}He shielding tensor of C_{60}^{10+} is a consequence of its strong aromaticity, as expected [26]. The high negative value of the ^{3}He NMR chemical shielding tensor for I_h C_{60}^- confirms its strongly antiaromatic character, which decreases when the symmetry is decreased to D_{3d}. Upon observing and comparing the ^{3}He shielding tensor values of I_h C_{60} and C_{60}^+, it is clear that cation generation has a huge effect on the aromaticity. However, the global minimum conformation of C_{60}^+ possesses weakly aromatic character, just like neutral fullerene.

Conclusions

Aromaticity and the JT effect are concepts of critical importance in chemistry, and although the connection between them is often overlooked, they have proven to be very useful for characterizing and interpreting the structures, stabilities, and reactivities of molecules.

The NICS values calculated in this work revealed that the magnetic fields inside C_{60} and C_{60}^{10+} are practically uniform throughout the interior cavity up to the walls, where local effects are decisive. Adding one electron to the LUMO of C_{60} while retaining an I_h geometry leads to the occurrence of intense antiaromaticity, whereas removing one electron from the HOMO orbital causes less pronounced paratropic character. It is important to remember that the JT-active species distorts to the LS, so the aromatic character cannot be fully gauged without including the JT distortion. The IDP model allows us to analyze the impact of JT distortion on the aromaticity. When the changes in the NICS values for C_{60}^- and C_{60}^+ along this particular path of distortion are monitored, it becomes clear that the antiaromaticity decreases with increasing deviation from

the HS to the LS point group. The anion C_{60}^- remains antiaromatic in the global minimum structure. In its global minimum conformation, C_{60}^+ has a similar aromatic character to neutral, non-JT-active C_{60}. In analogy to the benzene cation and anion [11], the JT effect acts to reduce the antiaromaticity, and thus represents a mechanism for lowering it. Substantial differences in the aromatic/antiaromatic behavior of the JT-active fullerene ions lead to different reaction pathways (i.e., aromatic species are prone to strongly electrophilic aromatic substitutions but show low reactivity in addition reactions), so the analysis of vibronic coupling and aromaticity along a distortion path is clearly important.

Computational details

The structures of C_{60}, C_{60}^{10+}, C_{60}^-, and C_{60}^+ were optimized by DFT calculations using the Amsterdam Density Functional program package, ADF 2010.01 [31–33]. The local density approximation (LDA) characterized by the Vosko–Wilk–Nusair (VWN) [34] parameterization was used for the symmetry-constrained geometry optimizations. An all-electron triple-zeta Slater-type orbitals (STO) plus one polarization function (TZP) basis set was used for all atoms. In all cases, the global minimum was confirmed by the absence of imaginary frequency modes.

NICS values and ^{3}He NMR chemical shifts were calculated at the B3LYP/6-311+G* level of theory using the Gaussian 09 W program package [35–38]. NICS parameters were calculated for ghost atoms located at the centers of the investigated molecules, as well as in the centers of the pentagon and hexagon rings and 1 Å above them. In order to obtain the full profile of spherical aromatic behavior, calculations of NICS parameters were performed from 0 to 5 Å, in steps of 1 Å, following the C_5, C_3, and C_2 symmetry axes of C_{60} and C_{60}^{10+}. NICS parameters for JT-active fullerenes were scanned along the IDP, following the C_3 and C_2 symmetry axes for C_{60}^- and the C_5 and C_2 axes for C_{60}^+. Calculations of ^{3}He NMR chemical shifts were done at the centers of the C_{60}, C_{60}^{10+}, C_{60}^-, and C_{60}^+ molecules.

The intrinsic distortion path

The basis of the IDP method [22–25] is to represent the distortion along the minimum energy path from the HS nuclear arrangement to the LS energy minimum conformation, projecting the geometry of the system onto the normal modes of the distorted configuration. Hence, the distortion, connecting the HS configuration with the LS structure, can be given as a superposition of all totally symmetric normal modes in the LS point group. In this model, the geometry of the LS energy minimum obtained from DFT calculations was chosen to be the origin of the configuration space, $\vec{R}_{\mathrm{LS}} = 0$. Every point on the potential energy surface can be represented by a $3N$-dimensional vector, N being the number of atoms, $\vec{R}_X$, using mass-weighted generalized coordinates relative to the origin. Within the harmonic approximation, it is possible to express $\vec{R}_X$ as a linear combination of N_{a1} totally symmetric normal coordinates in the LS:

$$\vec{R}_X = \sum_{k=1}^{N_{a1}} \omega_{Xk} \vec{Q}_k, \tag{1}$$

where ω_{Xk} are weighting factors that represent the contribution of the displacements along the different totally symmetric normal coordinates to $\vec{R}_X$; $\vec{Q}_k$ are mass-weighted totally symmetric normal coordinates, which are the eigenvectors of the Hessian obtained from the DFT frequency calculations performed for the LS minimum energy conformation. The corresponding eigenvalues are λ_k.

The energy of the nuclear configuration $\vec{R}_X$, E_X, relative to the LS energy minimum is expressed as the sum of the energy contributions of the totally symmetric normal modes:

$$E_X = \sum_{k=1}^{N_{a1}} E_k = \frac{1}{2} \sum_{k=1}^{N_{a1}} \omega_{Xk}^2 \vec{Q}_k^2 \lambda_k. \tag{2}$$

The force at any given point (X), $\vec{F}_{Xk}$, is defined as a derivative of the energy over Cartesian coordinates; at the HS point, this indicates the main driving force for JT distortion. The total force is represented as a vector sum of the individual forces:

$$\vec{F}_{X\mathrm{tot}} = \sum_{k=1}^{N_{a1}} \vec{F}_{Xk} = \sum_{k=1}^{N_{a1}} \omega_{Xk} \lambda_k \mathrm{M}^{1/2} \vec{Q}_k, \tag{3}$$

where $\mathbf{M}$ is a diagonal $3 \times 3N$ matrix with atomic masses in triplicate as elements (m_1, m_1, m_1, m_2, …, m_n), which enables the IDP from the HS to the LS point to be calculated exactly. Briefly, with the IDP model, we are able to quantify the contributions of all normal modes to the JT distortion, and their energy contributions to the JT stabilization energy (E_{JT}) and to the total force at the HS point. It should be pointed out that the IDP model is completely nonempirical (no fitting of experimental data is required) and exact within the harmonic approximation. One of the biggest advantages of the IDP model is that it allows the changes in the forces of the normal modes along the particular path of distortion (IDP) to be monitored, which provides further insight into what happens during the distortion.

Matlab scripts for the IDP analysis and for extracting the necessary data from the ADF frequency calculations can be obtained from the authors upon request.

Acknowledgments This work was supported by the Serbian Ministry of Education and Science (Grant No. 172035) and the Swiss National Science Foundation.

References

1. Hirsch A, Chen Z, Jiao H (2000) Angew Chem Int Ed 39:3915
2. Hirsch A, Chen Z, Jiao H (2001) Angew Chem Int Ed 40:2834
3. Chen Z, Jiao H, Hirsch A, Thiel W (2001) J Mol Model 7:161
4. Poater J, Solà M (2011) Chem Commun 47:11647
5. Chen Z, King RB (2005) Chem Rev 105:3613
6. Bühl M, Hirsch A (2001) Chem Rev 101:1153
7. Bean DE, Muya JT, Fowler PW, Nguyen MT, Ceulemans A (2011) Phys Chem Chem Phys 13:20855
8. Jahn HA, Teller E (1937) Proc R Soc Lond Ser A 161:220
9. Bersuker IB (2006) The Jahn–Teller effect. Cambridge University Press, Cambridge
10. Tsipis AC (2009) Phys Chem Chem Phys 11:8244
11. Andjelković LJ, Perić M, Zlatar M, Grubišić S, Gruden-Pavlović M (2012) Tetrahedron Lett 53:794
12. von Ragué Schleyer P, Maerker C, Dransfeld A, Jiao H, van Eikema Hommes NJR (1996) J Am Chem Soc 118:6317
13. Jiao H, von Ragué Schleyer P (1996) Angew Chem Int Ed 35:2383
14. Saunders M, Jimenez-Vazquez HA, Cross RJ, Mroczkowski S, Freedberg DI, Anet FAL (1994) Nature 367:256
15. Saunders M, Jimenez-Vazquez HA, Bangerter BW, Cross RJ, Mroczkowski S, Freedberg DI, Anet FAL (1994) J Am Chem Soc 116:3621
16. Saunders M, Jimenez-Vazquez HA, Cross RJ, Billups WE, Gesenberg C, Gonzalez A, Luo W, Haddon RC, Diederich F, Herrmann A (1995) J Am Chem Soc 117:9305
17. Saunders M, Cross RJ, Jimenez-Vazquez HA, Shimshi R, Khong A (1996) Science 271:1693
18. Shabtai E, Weitz A, Haddon RC, Hoffman RE, Rabinovitz M, Khong A, Cross RJ, Saunders M, Cheng PC, Scott LT (1998) J Am Chem Soc 120:6389
19. Bühl M, Thiel W (1995) Chem Phys Lett 233:585
20. Bühl M, Patchkovskii S, Thiel W (1997) Chem Phys Lett 275:14
21. Kleinpeter E, Klod S, Koch A (2008) J Org Chem 73:1498
22. Zlatar M, Brogg JP, Tschannen A, Gruden-Pavlović M, Daul C (2012) In: Atanasov M, Daul C, Tregenna-Piggott PLW (eds) Vibronic interactions and the Jahn–Teller effect. Progress in theoretical chemistry and physics, vol 23. Springer, Heidelberg, p 25
23. Ramanantoanina H, Gruden-Pavlović M, Zlatar M, Daul C (2013) Int J Quantum Chem 113:802. doi:10.1002/qua.24080
24. Gruden-Pavlović M, García-Fernández P, Andjelković LJ, Daul C, Zlatar M (2011) J Phys Chem A 115:10801
25. Zlatar M, Schläpfer C-W, Daul C (2009) The Jahn–Teller effect. In: Köppel H, Yarkoni DR, Barentzen H (eds) Fundamentals and implications for physics and chemistry, 97th edn. Springer Series in Chemical Physics. Springer, Berlin, p 131
26. Johansson MP, Jusélius J, Sundholm D (2005) Angew Chem Int Ed 44:1843
27. Zanasi R, Fowler PW (1995) Chem Phys Lett 238:270
28. Manini N, Dal Corso A, Fabrizio M, Tosatti E (2001) Phyl Mag B 81:793
29. Ceulemans A, Fowler PW (1990) J Chem Phys 93:1221
30. Swart M, Bickelhaupt FM (2008) J Comput Chem 29:724
31. SCM (2010) ADF 2010.01. Scientific Computing & Modelling NV, Vrije Universiteit, Amsterdam. http://www.scm.com
32. Guerra CF, Snijders JG, te Velde G, Baerends EJ (1998) Theor Chem Acc 99:391
33. te Velde G, Bickelhaupt FM, van Gisbergen SJA, Guerra CF, Baerends EJ, Snijders JG, Ziegler T (2001) J Comput Chem 22:931
34. Vosko S, Wilk L, Nusair M (1980) Can J Phys 58:1200
35. Frisch MJ, Trucks GW, Schlegel HB, Scuseria GE, Robb MA, Cheeseman JR, Scalmani G, Barone V, Mennucci B, Petersson GA, Nakatsuji H, Caricato M, Li X, Hratchian HP, Izmaylov AF, Bloino J, Zheng G, Sonnenberg JL, Hada M, Ehara M, Toyota K, Fukuda R, Hasegawa J, Ishida M, Nakajima T, Honda Y, Kitao O, Nakai H, Vreven T, Montgomery Jr JA, Peralta JE, Ogliaro F, Bearpark M, Heyd JJ, Brothers E, Kudin KN, Staroverov VN, Kobayashi R, Normand J, Raghavachari K, Rendell A, Burant JC, Iyengar SS, Tomasi J, Cossi M, Rega N, Millam JM, Klene M, Knox JE, Cross JB, Bakken V, Adamo C, Jaramillo J, Gomperts R, Stratmann RE, Yazyev O, Austin AJ, Cammi R, Pomelli C, Ochterski JW, Martin RL, Morokuma K, Zakrzewski VG, Voth GA, Salvador P, Dannenberg JJ, Dapprich S, Daniels AD, Farkas Ö, Foresman JB, Ortiz JV, Cioslowski J, Fox DJ (2009) Gaussian 09, revision A.1. Gaussian Inc., Wallingford
36. Becke AD (1986) J Chem Phys 84:4524
37. Perdew JP, Yue W (1986) Phys Rev B 33:8800
38. Perdew JP (1986) Phys Rev B 33:8822